JGR Oceans

RESEARCH ARTICLE
10.1029/2020JC016919

Climate-Based Emulator of Distant Swell Trains and Local Seas Approaching a Pacific Atoll

Laura Cagigal[1,2], Ana Rueda[2], Alba Ricondo[2], Jorge Pérez[3], Nicolás Ripoll[2], Giovanni Coco[1], and Fernando J. Méndez[2]

[1]School of Environment, University of Auckland, Auckland, New Zealand, [2]Departamento de Ciencias y Técnicas del Agua y del Medio Ambiente, Geomatics and Ocean Engineering Group, Universidad de Cantabria, Santander, Spain, [3]MetOcean Solutions, Meteorological Service of New Zealand Ltd. (MetService), Raglan, New Zealand

Key Points:

- A climate-based emulator of swell trains and local seas capable to generate multimodal wave conditions is presented
- An algorithm to isolate and parameterize swell trains is developed and waves are linked to large-scale climate patterns
- The validation of the reconstructed spectra against the hindcast confirms the capability to reproduce the historical ocean waves behavior

Correspondence to:
L. Cagigal,
lcag075@aucklanduni.ac.nz

Citation:
Cagigal, L., Rueda, A., Ricondo, A., Pérez, J., Ripoll, N., Coco, G., & Méndez, F. J. (2021). Climate-based emulator of distant swell trains and local seas approaching a Pacific atoll. *Journal of Geophysical Research: Oceans*, *126*, e2020JC016919. https://doi.org/10.1029/2020JC016919

Received 27 OCT 2020
Accepted 7 JUN 2021

Abstract Wave-induced flooding is a major coastal hazard for the low-lying atolls of the Pacific. These flooding events are expected to increase over time, which may cause significant coastal damage in some locations. Coastal flooding analysis (forensic or forecasted) is particularly challenging in these small islands due to the co-occurrence of several swells and local seas propagating in a complex configuration of archipelagos. Therefore, assessing the contribution of swells and wind seas on the flooding hazards that threaten the atoll islands requires the spectral characterization of the wave climate, since integrated wave parameters do not accurately represent the wave conditions in these environments. On the other hand, the relative short records of wave conditions, represent only a small fraction of the possible range of combinations that could produce a wave-induced flooding event. For these reasons, we propose the analysis of all the spectral energy arriving toward a study site, by isolating and parameterizing each swell train. Then, taking into account the link with large-scale climatic patterns (i.e., El Niño Southern Oscillation), we present a new multi-modal seas emulator capable of generating infinitely long time series of synthetic individual swell trains and seas. This new climate-based emulator allows a better understanding of swell behavior in the Pacific, and the generation of multimodal wave conditions to populate the historical records as a key point to perform robust coastal flood risk assessments considering climate variability.

Plain Language Summary Coastal flooding events generated by waves are a key issue for low-lying Pacific atolls. Those events are expected to increase over time due to climate change and in order to be prepared, it is important to study where those waves are generated. As those atolls are located in the middle of a large ocean, where concurrent waves approach from every direction, we need to use the wave spectrum which characterizes the distribution of energy at different directions and frequencies. We propose the analysis of Majuro, capital of the Marshall Islands, aggregating all the spectral wave energy surrounding the atoll into a "super-point". Then, we identify the local generated waves (i.e., seas) and the individual far field generated waves (i.e., swell trains), and find its link with large scale climatic patterns (i.e., El Niño Southern Oscillation). Knowing this link, we develop a climate-based emulator capable of generating infinitely long time series of synthetic swell trains and seas that maintain the same properties as the historical records. This new emulator allows a better understanding of swell behaviour, and the generation of multimodal wave conditions to populate the historical records in order to perform robust coastal flood risk assessments considering climate variability

1. Introduction

The general understanding of coastal inundation in the low-lying nations of the Pacific areas relates flooding to extreme water levels (i.e., astronomical tides, sea level variability) or tropical cyclones (Hoeke et al., 2013). Nevertheless, distant-source swells are less studied (Hoeke et al., 2013) and are one of the main causes of coastal flooding in the Pacific (Ford et al., 2018). After traveling thousands of kilometers (Snodgrass et al., 1966), swell dissipation results in wave set-up due to breaking waves and infragravity waves (Pomeroy et al., 2012), increasing the local impact when they reach the reef-lined coast. Furthermore, differently to tropical storms which may have more localized impacts, far-field swells can cause flooding damage among a large number of Pacific islands and atolls at the same time, as it happened in the inundation event of December 2008 (Hoeke et al., 2013).

Due to the complexity of these reef environments and ongoing climate changes, there is an increasing need for customized coastal hazards assessments and inundation forecast systems (Wandres et al., 2020; Winter et al., 2020). Although some studies indicate that low-lying atoll islands will adapt to increasing sea level rise (SLR) (Ford & Kench, 2015; Kench et al., 2015), it is expected that the frequency of inundation events associated to wave-driven (i.e., run-up and overwash) processes will increase over time (Cheriton et al., 2016). This means that for many atolls it will be impossible to live by the mid-21st century without persistent infrastructural damage and issues reaching freshwater resources (Storlazzi et al., 2018). Projections suggest that by the end of the century, the present 100 years return period of extreme sea levels will occur annually in most coastal areas (Vousdoukas et al., 2018). Furthermore, it has been demonstrated that at some locations, including the wave contribution to coastal flooding as the sea level rises, increases almost exponentially the average number of flooding days (Merrifield et al., 2014). The frequency and intensity of this wave contribution will ultimately depend on the local variability and trends of the hydrodynamic forcing (Reguero et al., 2019).

Pacific atolls, located in the middle of a large ocean basin, are generally affected from a local sea and a number of concurrent distant-source swells approaching from different directions. These swells are relatively persistent in direction and period, and have been historically used for navigation by what is called wave piloting, which consists on sensing the presence of land by reading how atolls and islands disrupt distant generated swells (Genz et al., 2009; Van Vledder, 2015). The aggregation of the full spectrum into single parameters, which may correctly account for the wave characteristics of uni-modal seas, often results in the loss of a significant amount of detail associated with these multi-modal seas (Portilla et al., 2015). Nevertheless, integrated bulk parameters (i.e., significant wave height, period and direction) remain commonly used, although the need of using the wave spectrum for describing complex sea states is becoming evident.

For these reasons, here we analyze all the spectral wave energy arriving toward a Pacific atoll, aggregating the information of six different points surrounding the study site to avoid the shadowing effects produced by its own land presence. In order to analyze the source and travel time of the distant source swells following the dispersion relationships of swells in deep oceans (Portilla, 2012), the full spectra has been partitioned following a watershed algorithm (Hanson & Phillips, 2001) to divide the sea and swell partitions and obtain its representative parameters: significant wave height (Hs), peak period (Tp), and direction (Dir). Then, an algorithm to isolate individual swell trains generated by a common source has been developed so that swell trains can be parameterized into: Hs_{max}, Tp_{max}, Dir, duration and damping coefficients for Hs and Tp. Those parameters have been then analyzed and linked with the seasonality and El Niño Southern Oscillation (ENSO) as the main driver of interannual variability in the Pacific Region (Philander, 1983).

With all the information obtained from the spectral analysis, the final goal of this work is to develop a new climate-based emulator of local seas and swell trains. The relative short historical record of the full multidimensional space contributing to total water level, results in historical observations of only a small fraction of all the possible range of conditions that could potentially lead to coastal flooding (Leonard et al., 2014; Marcos et al., 2019; Serafin & Ruggiero, 2014). To overcome the restrictions imposed by the lack of historical records, climate-based emulators have arisen as an alternative to reproduce synthetic time series of waves. Emulators allow to analyze long-term projections probabilistically, as infinitely long time series of hydrodynamic conditions can potentially be generated at a relatively low computational effort. Furthermore, emulators reduce the cost of using wave ensembles which in the last years have become a powerful tool to reduce (Wahl et al., 2012) and assess (Vitousek et al., 2017, 2021) the uncertainty of coastal hazard predictions due to wave climate variability.

Although there have been a number of wave climate emulators developed in the past years (Anderson et al., 2019; Antolínez et al., 2016; Cagigal et al., 2020; Callaghan et al., 2008; Lucio et al., 2020; Rueda et al., 2017), this is the first one to our knowledge to deal with the emulation of concurrent seas and individual swell trains with its own duration and characteristics over time. This kind of emulation approach is especially suited for islands and atoll environments where concurrent swells can reach the study site from many different directions but could also be used at any location in which distant source swells are present.

The paper is organized as follows. Section 2 presents the atoll and the wave data chosen for this study. Section 3 describes the analysis of the wave spectra, its link with seasonality and ENSO variability and the

methodology followed to develop the climate-based emulator. Section 4 presents the results obtained from the emulation process and the spectral validation against hindcast data. A discussion and concluding remarks are presented in Sections 5 and 6 respectively.

2. Study Site and Wave Data

Although this analysis could be of interest to any Pacific low-lying atoll, Majuro has been chosen as our study site. Majuro is a low-lying atoll located in the central Pacific, formed by over 60 islands with a total land area of about 10 km^2, that enclose a large lagoon of 300 km^2 (Gesch et al., 2020). It is the capital of the Republic of the Marshall Islands and accounts for 27,797 residents, 52% of the national population, which is mostly concentrated on the Delap-Uliga-Djarrit (D.U.D.) area in the eastern side of the atoll (Ford et al., 2018). Due to continuous land reclamation in order to accommodate the very high density populated D.U.D. area, the hardened shoreline of Majuro will be unable to adjust to future SLR scenarios (M. Ford et al., 2018), which are projected to be greater than the global average (Gesch et al., 2020; Spada et al., 2013). It is also predicted that for 1 m SLR scenarios, the threshold Hs to produce overtopping in Majuro will decrease by a 71% (Beetham & Kench, 2018).

Even without accounting for the future effect of SLR, Majuro, with much of its land area at less than 3 m above the mean sea level, is at present an atoll very prone to flooding. The analysis of 18 historical flooding events in Majuro carried out in Ford et al., (2018) classifies the events into five different types: wave-driven inundation from distant swells, inundation from tropical storms and typhoons, from elevated water levels, from swell penetration into the lagoon and from waves generated inside the lagoon. Distant generated swells from the north have resulted in costly impacts for the D.U.D. while those generated in the southern Pacific, although smaller in magnitude, have also caused damage to singular infrastructures located in the southern rim, as it is the airport. These events are not necessarily associated with strong local winds and high sea levels are not required for this flooding type to cause large damages.

In this study, the ocean waves have been characterized using directional wave spectra from a model hindcast from 1979 to 2019 developed by the Australian Bureau of Meteorology and the Climate Science Center (CSIRO) and known as Center for Australian Weather and Climate Research wave hindcast (Durrant et al., 2014; Smith et al., 2020). The numerical model used for this hindcast is WAVEWATCH III (Tolman, 1991) forced with winds from the Climate Forecast System Reanalysis (CFSR) developed by the National Center for Environmental Prediction (NCEP). This hindcast provides partitioned wave parameters at a global resolution of 0.4° with a finer resolution of 4′′ and 10′′ on the Australian and south pacific regions. Nevertheless, for the specific case of spectral data, it is provided at 10° resolution in the global grid and at 0.5° for Australia and the Pacific region. Figure 1a shows the area of interest that covers both Majuro atoll and Arno atoll, which in the past, due to them being closely located and intervisible, have been considered as a single navigation target (Genz et al., 2009). The hindcast points used as input, shown in Figure 1b, give spectral wave energy information among 29 exponentially spaced frequencies from 0.038 to 0.5 Hz and 24 directions discretized every 15°.

3. Methodology: Emulator Development

The general methodology followed for the analysis and the development of the climate-based emulator of distant source swells and local seas is shown in Figure 2. The starting point of the methodology is the wave hindcast spectral information at the six different locations shown in Figure 1b, and then aggregated into a "super-point" (Figure 1c) for which wave partitioning is performed (Figure 1d). From there, the methodology is divided in two different branches. Due to the different behavior of seas and swells, they are treated independently and later on integrated by spectral reconstruction, considering that they respond to the same large-scale patterns at seasonal and interannual scales. Sections 3.1–3.3 correspond to the development of the swell branch while Section 3.4 focuses on the seas.

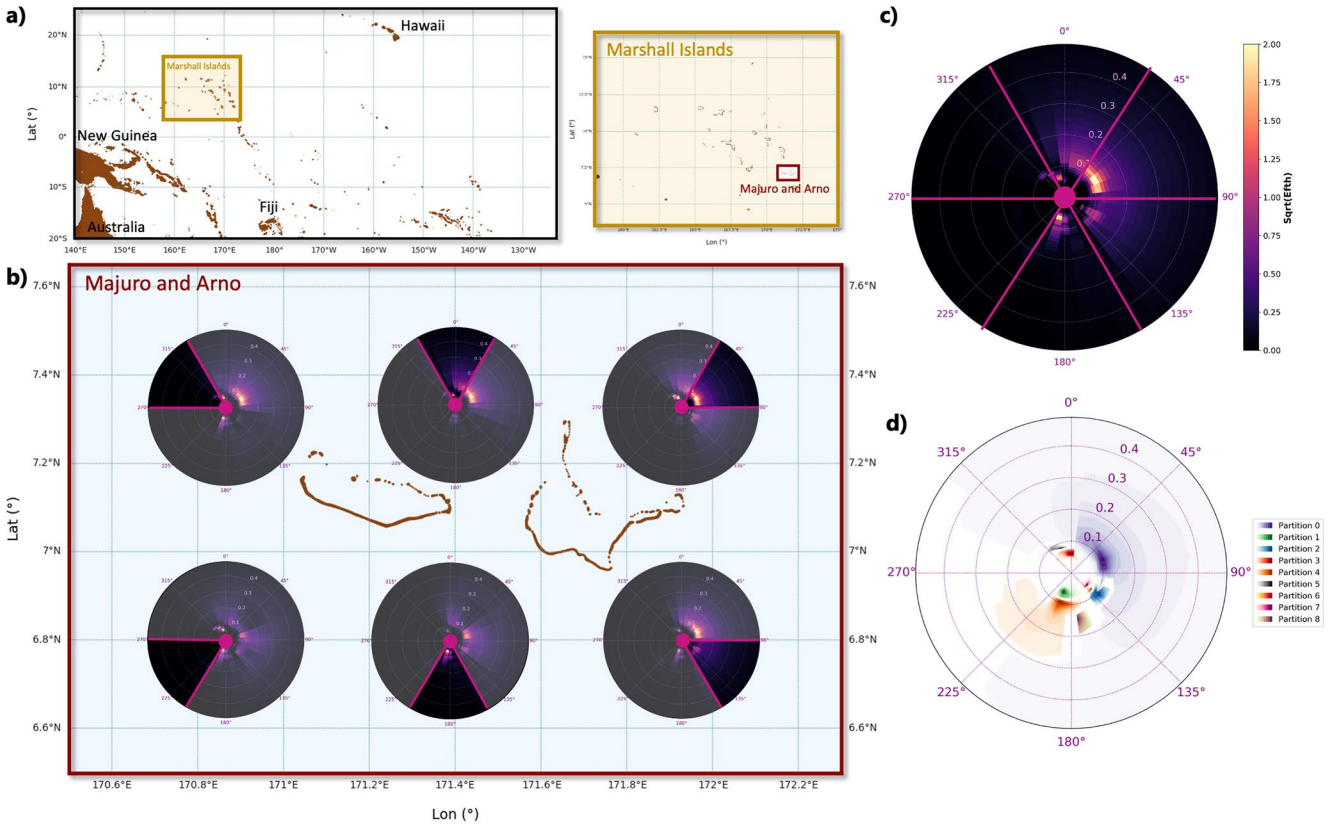

Figure 1. (a) Study site location. (b) Wave spectra at the six locations surrounding Majuro and Arno atolls where data is available. (c) Aggregated wave spectra following the "super-point" methodology. (d) Wave partitioning of the spectra shown in (c).

3.1. Definition of the Super-Point

In large ocean basins as the Pacific, sea states are the result of superposing a number of wave trains that propagate from different direction and frequencies (Delpey et al., 2010). Generally, the spectrum is characterized by a locally generated sea and different swells generated by distant storms. The number of concurrent swells is highly dependent on the location, with the Pacific and tropical areas being the ones with larger numbers (Jiang, 2019).

In this work, in order to account for all the possible sources of energy and to avoid the shadowing effect due to land presence, the first step consists on defining a "super-point," which aggregates the spectral energy of the six different hindcast points shown in Figure 1b surrounding Majuro and Arno atolls. This virtual super-point informs of all the energy approaching the area of interest every hour. The construction of this super-point is based on the directional sectors shown in Figure 1b, so every hindcast point represents a 60° directional sector of the super-point spectra (Figure 1c).

Once the energy is aggregated, the next step is a spectral partitioning, a technique first introduced by Gerling (1992) to define the parts of the spectrum that correspond to a system of waves from the same meteorological event (Portilla et al., 2009). The spectral partitioning has been performed using WAVESPECTRA (https://github.com/metocean/wavespectra), a python library for ocean waves that uses the watershed algorithm implemented in WAVEWATCH III first developed by Hanson and Phillips (2001) and as described in Tracy et al., (2007). The library allows the user to define the maximum number of swell partitions to consider and this limit has been set up to eight. In this case, introducing a larger number, results in partitions with almost no energy. The other parameters to define are the wave age factor, which amplifies the size of the area in the spectrum under the direct influence of the wind, and the wind cut, that corresponds to the energy fraction of the partition under the previously defined wind influence area for the partition to be considered wind sea instead of swell (Tracy et al., 2007). The default implemented values are 1.7 for the wave

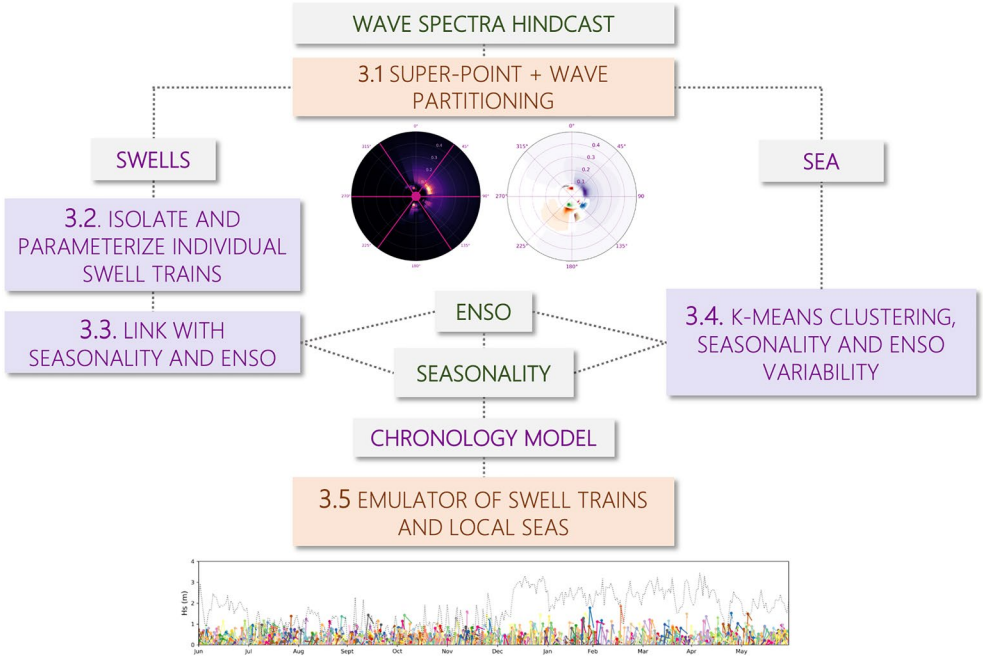

Figure 2. Methodology for the emulation of swell trains and local seas. Lower panel corresponds to the final output of the methodology presented.

age factor (Tracy et al., 2007) and 0.333 for the wind cut, nevertheless these limits shown an erratic switch between the sea and swell partition at our study site, and for this reason, we have analyzed different pairs of these values and finally kept the age factor to 1.7 while changing the wind cut to a factor close to 0. This way the continuity of the sea partition is maintained over time while truly separating distant source swells from the more locally developed seas or young swells still influenced by the wind. In our study site, the sea partition is forced by the almost constantly blowing trade winds from the north-east direction, and therefore is characterized by an almost constant direction and period (see Figure 3b), with large mean directional spreading, typical for wind sea waves (Portilla et al., 2015).

With this configuration, the spectral partitioning is obtained, and an example is shown on Figure 1d (the different partitions are represented by different colors). For the partitioned spectra, we can then obtain the bulk Hs, Tp, and Dir for each partition, which are the parameters used from now on to isolate and parameterize the different swell trains.

3.2. Swell Trains: Parameterization

Wave partitions obtained from WAVESPECTRA are classified into a sea, and a number up to eight swells sorted according to their energy. Therefore, those partitions are not necessarily associated to the same meteorological event over time. This section focuses only on the swell partitions, as the sea will be treated differently, and its analysis will be presented in Section 3.4. Different ways of associating swell partitions over time and space to a common source have been proposed in the literature (Aarnes & Krogstad, 2001; Delpey et al., 2010; Devaliere et al., 2009; Hanson & Phillips, 2001; Jiang, 2019; Kpogo-Nuwoklo et al., 2014). These methodologies can be divided on those that track the waves based on the dispersion relationship by analyzing the source time and location from every partition group and then verifying those that correspond to the same generating event (Aarnes & Krogstad, 2001) or those that track partitions developed from known sources (Delpey et al., 2010). Nevertheless, these methods only work for very far generated swells and lead to gaps making them not applicable for a comprehensive analysis of swell fields (Delpey et al., 2010). The other methodologies are the ones focused on using the continuity of the local bulk partitioned parameters in the spatial two dimensions space (Devaliere et al., 2009; Jiang, 2019) or over time (Hanson & Phillips, 2001; Kpogo-Nuwoklo et al., 2014).

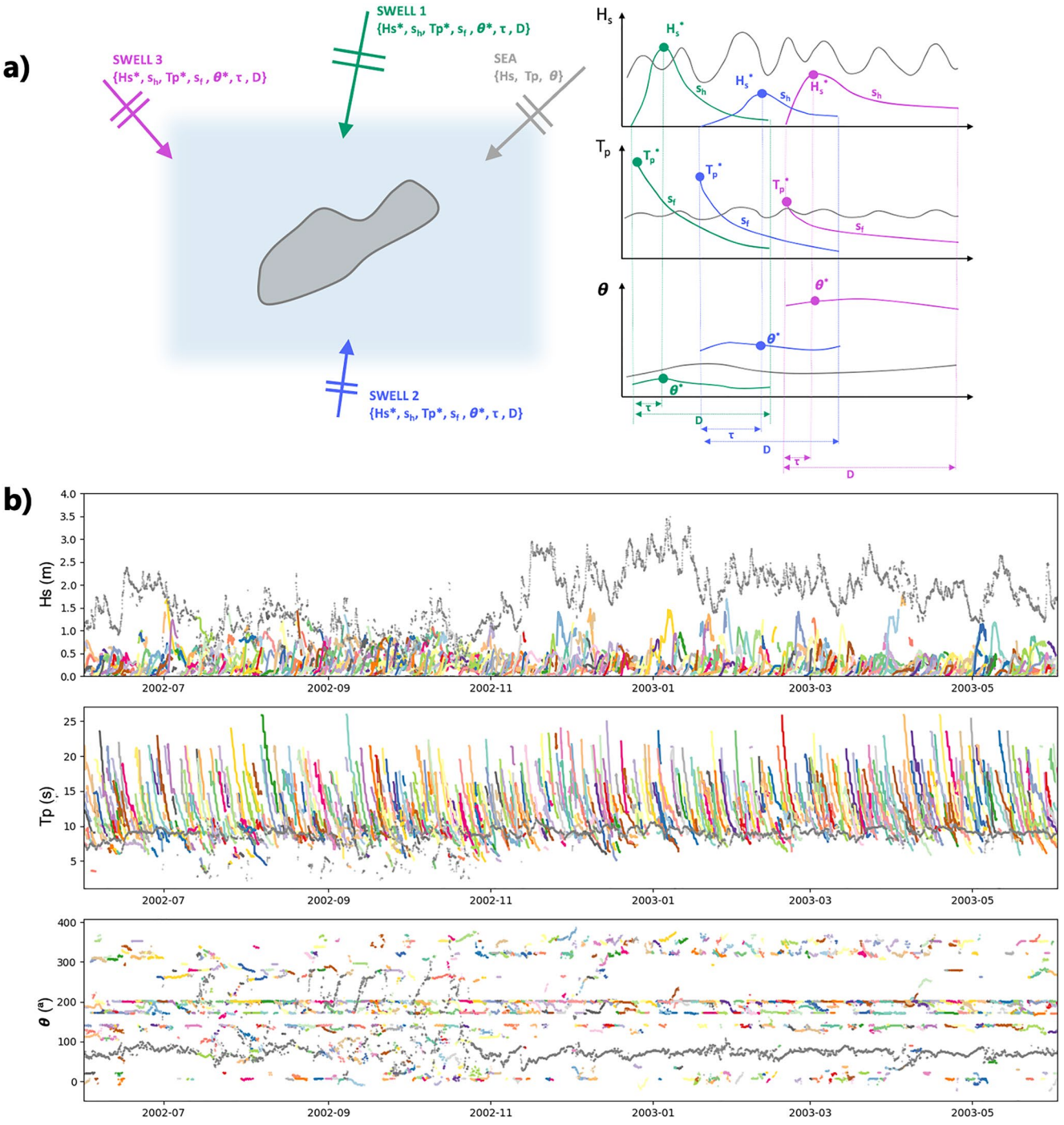

Figure 3. (a) Sketch representing a hypothetical system of three swells and one sea and its representative parameters: Hs, Tp, and Dir. (b) Time series of sea (gray) and isolated swell states (colors) for Hs (top), Tp (middle), and Dir (Bottom). Parameterization of each swell (right).

Here, we present a new tracking algorithm based on the time series of the local bulk partitioned Hs, Tp, and Dir. The algorithm consists on finding for each time step and partition, the closest partition in the following time step in terms of its bulk parameters. The closest partition is found by calculating the distance to the following time following Equation 1. For these calculations, the bulk parameters are previously normalized with the percentile 99.9 and 0.1 for the Hs and Tp and dividing the direction by π as in Camus et al. (2011).

$$\text{DISTANCE} = \sqrt{\left(\text{H}_{t+1} - \text{H}_t\right)^2 + \left(\text{Tp}_{t+1} - \text{Tp}_t\right)^2 + \left(\text{Dir}_{t+1} - \text{Dir}_t\right)^2}. \quad (1)$$

For the algorithm to work, we do also need to define a threshold for which we assume the distance is large enough for a partition to be part of the same swell train. For this reason, we have introduced a coefficient $\max D = \sqrt{N * \text{Perc}^2}$., where N is the number of variables introduced in the distance equation (3 in this case) and Perc corresponds to the maximum simultaneous change for all the variables (8% in this case). Furthermore, we have introduced additional thresholds to Hs and Tp, so that Tp can only decrease over time for each swell train by a maximum of a 25% and the variation in Hs can be up to a 20% from time to time, both increasing and decreasing. When any of the previous thresholds are not met, we let the algorithm to try and find continuity of the swell train in the following 15 h, as sometimes gaps on the partitions are observed, and if continuity is still not found, we start with a new swell train. All these limiting factors have been obtained through an iterative trial and error process, a commonly used practise for obtaining parameters associated with tracking algorithms (Hanson & Phillips, 2001; Jiang, 2019). The optimization has been made mostly by means of visual inspection of the results obtained and would probably need to be re-optimized for application at a new location.

Following the algorithm proposed, Figure 3b shows the swell trains obtained for a year as an example. Each color corresponds to one swell train in terms of Hs, Tp, and Dir. Gray color corresponds to the sea partition. As expected, generally the swell trains are characterized by an Hs that grows until it reaches a peak and then decays, an always decreasing Tp, and an almost constant Dir over time.

Every swell train, is then parameterized by means of the following seven parameters: Maximum Hs (Hs*), slope of the linear fit from Hs* to the end of the swell event (s_h), minimum peak frequency (Fp*), slope of the linear fit of Fp (s_f), direction at the instant of Hs* (Dir*), duration (D) of the swell train in hours and hours until Hs^* (τ). For simplicity, in the linear fitting process we work with Fp instead of Tp (Fp = 1/Tp). A sketch showing the different parameters of concurrent sea and swell events is presented on Figure 3a.

For the isolated swell trains, we use the dispersion characteristics of ocean waves to obtain the source and travel time of each of the different events following Equations 2 and 3 (Hanson & Phillips, 2001; Portilla, 2012):

$$t_0 = \frac{-b}{s_f}, \quad (2)$$

$$d = \frac{g}{4\pi s_f}, \quad (3)$$

where s_f is the slope of the linear fit of the frequency (F_p), t_0 corresponds to the travel time, d corresponds to the distance to the source and b corresponds to the intercept of the linear fit associated with the peak frequency. Due to storms being dynamic events with large dimensions, it is not realistic to define them with a unique point, and therefore the uncertainties associated with the linear fit of the peak frequency need to be analyzed (Portilla, 2012). For this purpose, we have obtained the 98% confidence intervals of the linear fit so that both travel time and distance to the source are defined within an interval. Dots in Figure 4 show the mean location points for all the swells arriving to Majuro, whereas the color refers to the distance range obtained from the 98% confidence analysis. Only swell trains with an uncertainty of less than 1,500 km are plotted and used for the travel time contour plot in the background, where numbers refer to the mean travel time in days needed for a swell to reach the study site. As we are using this analysis for a general understanding of the generation areas of swells approaching the study site, further uncertainties associated with the direction (Portilla, 2012) are not taken into account, and distances are calculated among the great circle of the mean swell direction.

Figure 4 confirms that waves approaching Majuro are generated across the whole Pacific and reiterates the importance of using the directional wave spectra against bulk parameters in order to capture the energy approaching from every direction. As observed from this analysis, the predominant swells from the South-

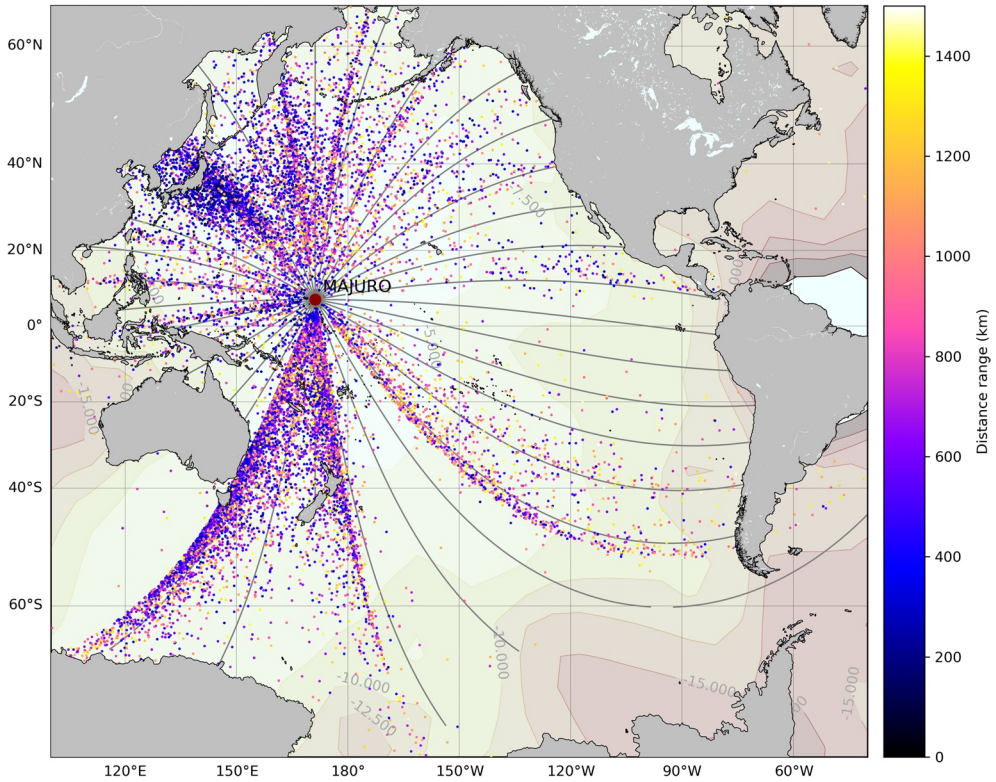

Figure 4. Source and travel time of distant source generated swells approaching Majuro atoll.

ern Hemisphere are generated in the area surrounding Australia and New Zealand, while for the Northern Hemisphere most swells are generated in the north west close to Japan. There is a notable gap of swells approaching from south eastern directions mostly due to the blocking produced by a number of small atolls and land presence close to the study site.

3.3. Swell Trains: Seasonality and ENSO Variability

The final goal of this study consists not only of analyzing the characteristics of swells approaching Majuro, but to develop a new multimodal seas emulator capable of generating long time series of hydrodynamic conditions for probabilistic assessments of coastal hazards. It is thus important that the synthetic time series are capable of reproducing the seasonal and the interannual variability, which in this area is linked to ENSO.

Analyzing the number of swell trains triggered every month of the year for every direction discretized every 10°, and the particular characteristics of the parameters Hs*, Fp*, D, and τ, provides insights on characteristic patterns. Figure 5 aggregates all the information and shows the mean and 95% percentile characterizing each variable and cell. When looking at the mean number of swells per year, it is clear that there is a predominant probability of swells approaching Majuro from 170° to 210° over the year, which corresponds to the New Zealand and Australia generation area, as was also observed in Figure 4. Nevertheless, during the months of November–March that correspond to the boreal winter, the swells are predominantly coming from northern directions, while the boreal summer (i.e., June–November) concentrates most of the swells coming from the south. The characteristics of these swells are very different. The ones from the north are generally characterized by relatively larger Hs*, lower Fp* (i.e., larger Tp) and shorter durations, while the longest swells, although with a small Hs*, are the ones approaching Majuro from the Southern Hemisphere. This is due to the distance source of generation in the southern Pacific and the shadowing effect of waves by a large number of islands (Ford et al., 2018).

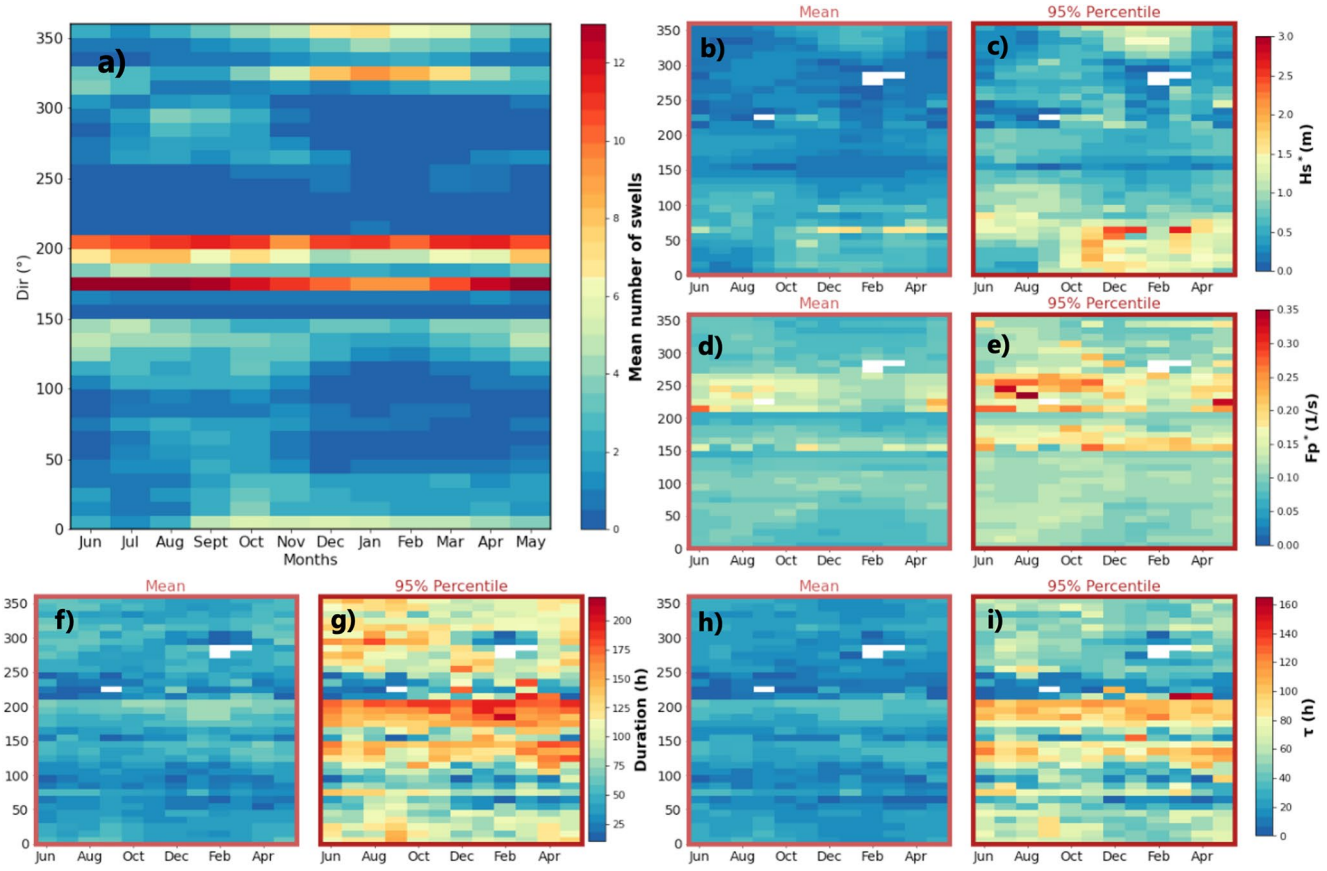

Figure 5. (a) Mean number of swells, mean and 95 percentile associated to Hs* (b, c), to Fp* (d, e), to D (f, g) and to τ (h, i) for every month (*x*-axis) and direction discretized every 10° (*y*-axis).

Although the number of swells shown in Figure 5 captures the seasonality along the year, the interannual variability is dominated by ENSO, with teleconnections affecting weather all over the world (Philander, 1983). In the particular case of the Pacific, a positive correlation is found between the Niño three index and extreme Hs (Izaguirre et al., 2011) and wave power (Reguero et al., 2019). For this reason, the differences between El Niño and La Niña years should also be taken into account in any wave emulator developed for the area.

To account for the modulation on the number of swells produced by ENSO, we use the Annual Weather Types (AWTs) based on sea surface temperature anomalies (SSTA) proposed in Anderson et al. (2019). These AWTs are constructed by averaging the SSTA in the equatorial Pacific and defining Hovmöller diagrams (Hovmöller, 1949) beginning in June and ending the following May to preserve the boreal winter variability. The different years, represented by its first three principal components, are clustered into six different AWTs that group positive and negative anomalies of SSTA in the eastern Pacific characteristic of El Niño and La Niña respectively. Further details in the construction of the AWTs and the data used can be found in Anderson et al. (2019).

The AWTs time series from 1980 to 2016 are shown on the upper left panel of Figure 6 and the representative Hovmöller diagram of the centroid of each AWT is shown in the upper right panel. ENSO events represented on the time series correspond to very strong (ONI > 2) and strong (ONI > 1.5) El Niño and strong (ONI < −1.5) and Moderate (ONI < −1) La Niña years. AWT1 is therefore representative of El Niño events with positive SSTA located in the eastern pacific, while La Niña is presented by AWT6 with negative SSTA.

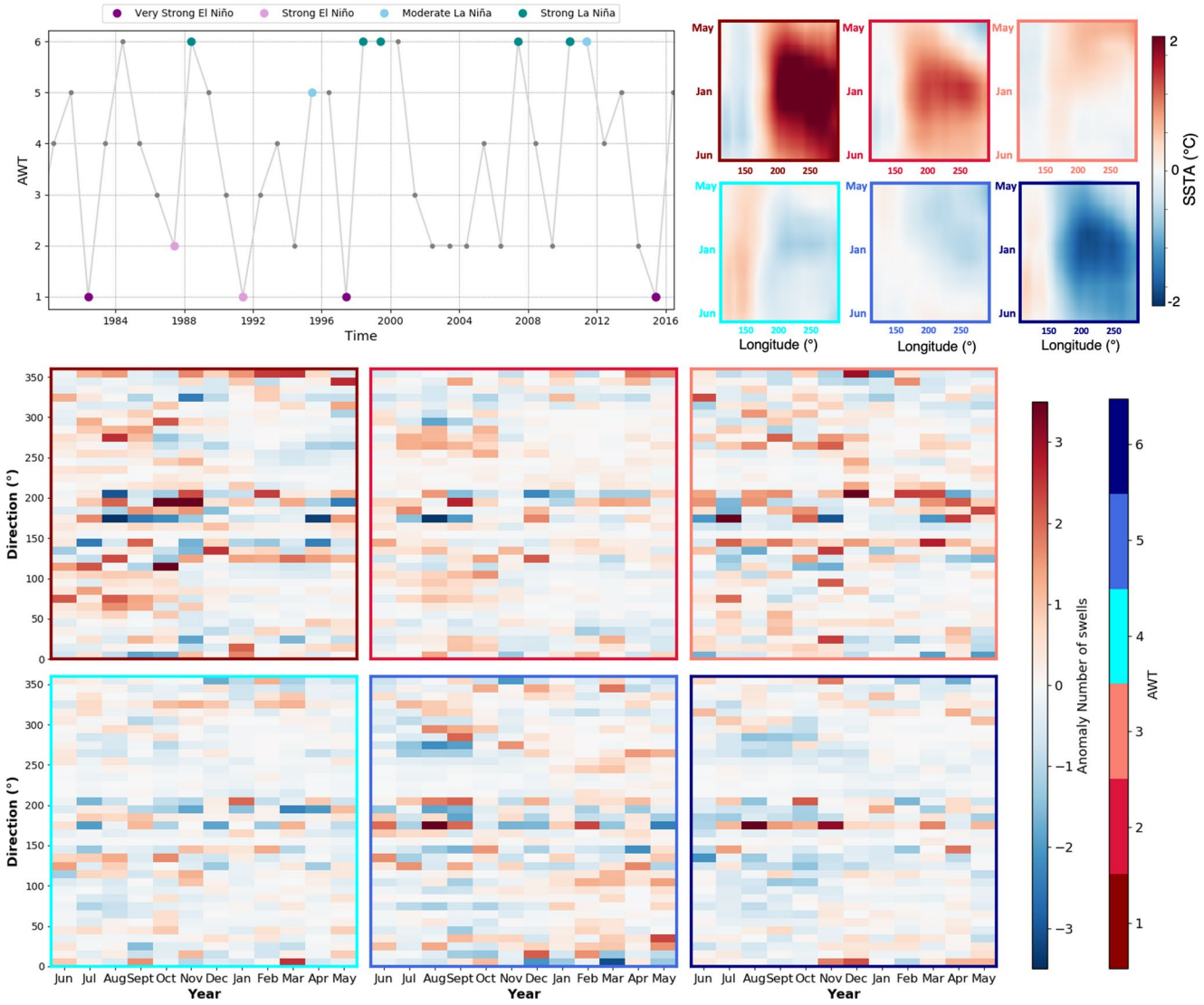

Figure 6. Time series of AWTs and representative Hovmöller diagram of the centroid of each cluster (upper panels). Anomaly on the number of swell trains associated to each AWT (lower panel). AWTs, Annual Weather Types.

The anomaly of the number of swells for each AWT is shown on the lower panel of Figure 6. Important differences are observed when comparing different AWTs. AWT1 (i.e., El Niño) is characterized by a general increase in the number of swells, especially from the northern and eastern directions and a decrease in the number of swells from southern directions. AWT6 (i.e., La Niña) is characterized by a general lower number of swells throughout the year with some increases in the southern directions.

3.4. Seas

The sea component obtained from the partitioned super-point is analyzed and treated independently in this study, as the behavior is different and the analysis of isolating and parameterizing distant-source swell trains would not be applicable. Figure 7a shows the Hs, Tp, and Dir associated to the sea partition from 1979 to 2018, which is characterized by large Hs, a mean Tp of 9 s and a predominant eastern Dir, triggered by the trade winds. These wave parameters have been clustered into 36 groups following a K-Means clustering technique (KMA, Hastie et al., 2001). The centroid of the groups is represented in Figure 7b by its Hs (background color), Tp (arrow color) and Dir (arrow). The box color corresponds to the KMA group as in the upper panel. The seasonality of these groups is represented in Figure 7c, where DJF stands

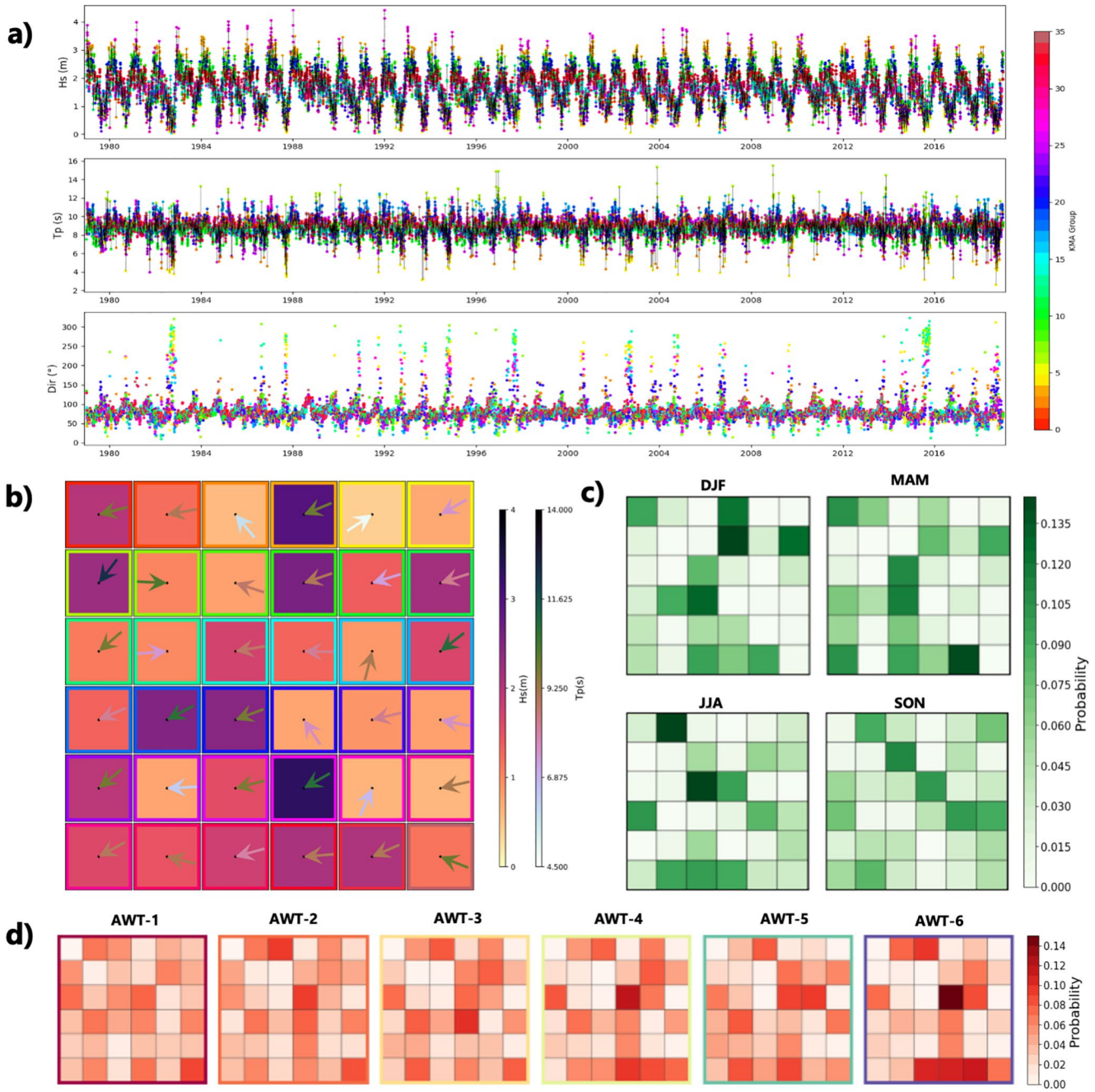

Figure 7. Hindcast seas analysis. (a) Time series of Hs, Tp, and Dir and KMA cluster in colors, (b) Clustering centroids represented by Hs (background color), Dir (arrow) and Tp (arrow color). Box color corresponds to the KMA group in panel (a). (c) Probability of each KMA cluster conditioned to the different seasons. (d) Probability of each KMA cluster conditioned to the different AWTs. AWTs, Annual Weather Types; KMA, K-Means clustering technique.

for December-January-February, MAM for March-April-May, JJA for June-July-August and SON for September-October-November.

Looking at these clusters, it is easy to see how the most probable groups are associated with eastern directions, which also account for the largest Hs and longer periods, while the southern and western wind sea waves are generally smaller and more locally generated (i.e., smaller periods). Although the predominant direction of the seas is eastern, there is also some seasonality present, as during the boreal winter the trade winds northeast directions are more common than during the rest of the year, when the direction is more

eastern and south-eastern (Genz et al., 2009). Also, the boreal summer is the season that accounts for most of the southern and south-western seas arriving toward Majuro.

Same as for the swells, interannual variability is also present in the sea partition, which has been analyzed based on the previously defined AWTs. Results associated to the probability of occurrence of each of the 36 clusters relative to the AWT are shown in Figure 7d, which shows an inter-annual variability among the different AWTs that would be consequently included in the emulation process. Differently than for the swells, which were more frequent during El Niño years, the seas are not especially more intense, as during El Niño trade winds are weaker (Timmermann et al., 2018).

3.5. Development of the Emulator

With all the wave parameters gathered, and its seasonality and link with ENSO, a new climate-based emulator of swell trains and local seas is developed, able to generate long term time series of multivariate sea states. Although the emulation process of the swell trains and local seas follows a different path, they will both be forced by the same large scale AWTs and seasonality, so that they can ultimately be put together.

The first step is generating the synthetic time series of AWTs, which is accomplished by means of an autoregressive logistic regression model (ALR, Guanche et al., 2014), fitted with a second order Markov chain (Anderson et al., 2019). This allows to generate 50 simulations of independent AWT chronologies that correctly reproduce the persistence, transition and probability of occurrence of ENSO during the hindcast period. The sequences are then converted to the representative three principal components by means of a Gaussian Copula (Ben Alaya et al., 2014) previously fitted for each AWT (for further details refer to Anderson et al., 2019).

An ALR model is also used to drive the chronology of the 36 KMA clusters defined for the sea partition in Section 3.4. In this case the ALR model is forced not only with a Markov chain, but also with the first three principal components representative of the AWT and the seasonality. This methodology has been previously used for generating synthetic daily chronologies in different applications using different covariates (Anderson et al., 2019; Antolínez et al., 2016; Cagigal et al., 2020). The seasonality and the KMA cluster probabilities associated to the different AWTs are maintained in the synthetic series, in addition to the probability of occurrence and the transition probabilities within clusters.

In order to resample from the synthetic KMA cluster and obtain the correspondent Hs, Tp, and Dir capturing the joint probability between variables, a Gaussian copula is previously fitted for each of the 36 clusters. Gaussian copulas have been proved to correctly deal with multivariate problems (Ben Alaya et al., 2014; Rueda et al., 2017). For this purpose, the different variables have been previously fitted to a Kernel distribution, which has a small capability of extrapolation while mostly maintaining the historical distributions. The distributions are then transformed to a normal, so that the dependencies in the Gaussian space are modeled by a matrix of Spearman's correlation coefficients. This way we are able of constructing the synthetic time series of sea parameters by randomly resampling a set of Hs, Tp, and Dir from the Gaussian copula.

For emulating the swell trains, we follow a different approach based on the number of swell events generated every month, for each direction and AWT. Once the synthetic AWT is known, the number of generated events for each direction and month is randomly obtained on a month by month iterative process. In order to control the total number of events generated each month and generate synthetic numbers coherent with historical values, it is important to take into account the correlation among the number of events associated to the different directions. To accomplish the simulation of the number of events while accounting for the correlation, we use a multivariate Poisson method, which is a generalization of the univariate case in order to incorporate correlation. The method consists on simulating multivariate normal data and converting them to obtain a correlation matrix and Poisson vector, which allows for the generation of a number of events with positive or negative correlations (details can be found in Yahav & Shmueli, 2007).

Once we have the random number of events from the multivariate Poisson for each of the 432 cells (i.e., 12 months and 36 directions), we resample back to the six swell parameters (i.e., direction is not included, as it will be characterized within the 10° cell range) that were defined during the parameterization process in Section 3.2 to reconstruct each swell train. To capture the joint probability between the six parameters,

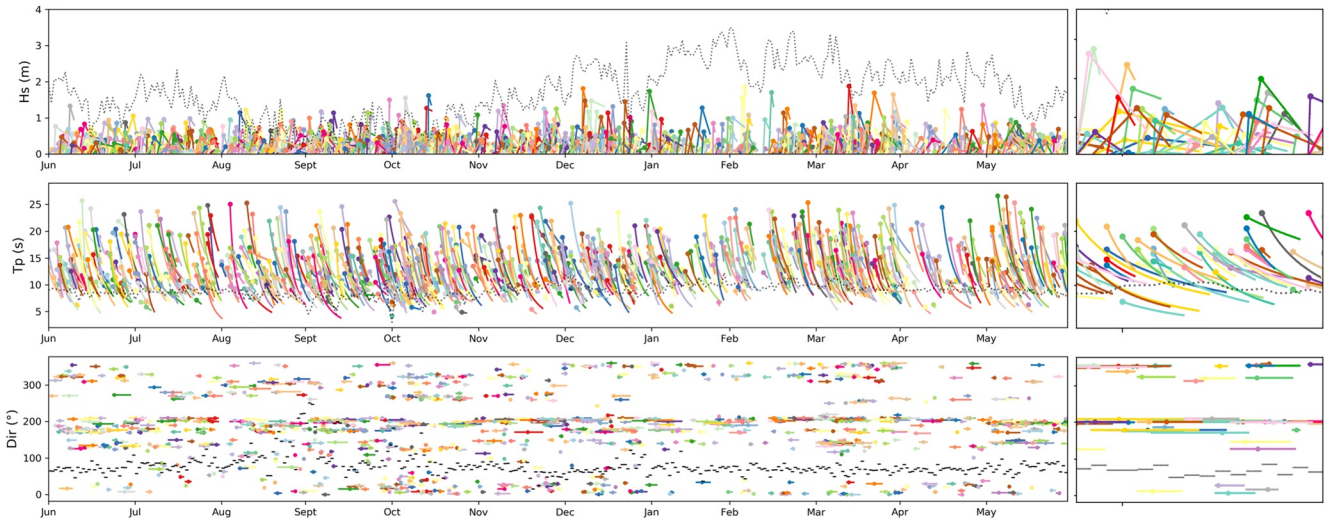

Figure 8. Emulated time series of sea (gray) and isolated swell states (colors) for Hs (top), Tp (middle), and Dir (bottom). A zoom of a smaller time period is shown on the right to better appreciate the shape of the individual emulated swell trains.

we fit a Gaussian copula for each cell and randomly resample a set of variables for each of the number of events obtained from the multivariate Poisson. For the direction, a random number from the cell interval discretized for every degree is assigned to the swell train, which will have its starting hour also randomly assigned within each month. Knowing the six parameters, the direction and the starting day of the month is enough to be able to obtain synthetic swell trains throughout the year, which takes into account the seasonality and the ENSO behavior.

4. Emulator Application and Spectral Validation

Building an emulator as in Section 3.6 allows for the generation of as many realizations of wave climate as desired for a specific application. For this study, 50 h simulations of swell trains and seas, with each simulation being 120 years long, have been obtained. Figure 8 shows the outputs for one of the emulated years as an example. Same as in Figure 3, the evolution over the year associated to the sea partition is shown in gray in Figure 8 and the different swell trains in colors. As observed, the shapes of the emulated Hs, Tp, and Dir have been reconstructed with the six parameters from the copula to obtain realistic swell trains.

Hs is characterized by a linear enhancement from zero until Hs* is reached after τ hours and a subsequent decay s_h. The Tp shown is the inverse of the peak frequency, obtained from Fp* and increasing at a rate s_f for the duration of the swell train. The direction randomly derived from the cell range, is constant over the duration of the swell train. For the sea, the daily values obtained from the copulas associated to each KMA cluster have been resampled to hourly values by interpolating Hs and Tp and leaving the direction constant for each day.

In order to validate the performance of the multimodal emulator proposed, the next step consists in reconstructing the different swells and sea at each hour into a theoretical spectrum, discretized with the same frequencies and directions as the input hindcast from CSIRO for comparison. For this purpose, each partition has been reconstructed as unimodal, so that the final multimodal spectra can be obtained by the aggregation of the unimodal spectra. The frequency-direction reconstruction $\left(S\left(f,\theta\right)\right)$ has been obtained following Equation 4, where $S(f)$ corresponds to the one-dimensional wave spectrum, $D(\theta)$ to the directional distribution, and n to the number of partitions every hour.

$$S\left(f,\theta\right) = \sum_{i=0}^{n} S_i\left(f\right) \cdot D_i\left(\theta\right). \tag{4}$$

The one dimensional wave spectrum has been fitted to a JOint North Sea WAve Project (JONSWAP) spectrum (Hasselman et al., 1973) using the formulation in terms of Hs and Tp (Goda, 1999) as in Equations 5–7. The

JONSWAP peak enhancement factor (γ) has been obtained from an empirical relationship between the peak and mean period as in Equation 8, where $a = 1.411$ and $b = -0.07972$. For the reconstruction process, a mean $\gamma = 1.2$ has been obtained for the sea partition in the hindcast, and based on the direction discretized every 10°, a mean γ value has been obtained for each swell direction with values ranging from 43.21 to 71.33.

$$S(f) = B_J \cdot H_s^2 \cdot T_p^{-4} \cdot f^{-5} \cdot \exp\left[-1.25 \cdot \left(T_p \cdot f\right)^{-4}\right] \cdot \gamma^{\exp\left[-\left(T_p \cdot f - 1\right)^2 / 2 \cdot \sigma^2\right]}, \tag{5}$$

$$B_J \approx \frac{0.06238}{0.23 + 0.0336 \cdot \gamma - 0.185\left(1.9 + \gamma\right)^{-1}} \cdot \left[1.094 - 0.01915 \cdot \ln\left(\gamma\right)\right], \tag{6}$$

$$\sigma = \begin{cases} 0.07 : f \leqslant f_p \\ 0.09 : f > f_p \end{cases}, \tag{7}$$

$$\frac{T_p}{T_{m02}} = a \cdot \gamma^b. \tag{8}$$

For the directional distribution, $D(\theta)$, a cosine expression (Mitsuyasu et al., 1975) has been used as in Equation 9, where θ_m is the mean direction of the partition, Γ is the gamma function, and s is a parameter that controls the directional width (Kuik, 1988), which depends on the directional spread (σ_θ) of each partition as in Equation 10. This directional distribution is defined so that Equation 11 is met. For this purpose, same as for γ, the parameter σ_θ has been obtained from the hindcast values for the sea partition $\left(\sigma \mid \theta = 30.8\right)$ and for the swells depending on the direction discretized every 10°, with a range from 4.66 to 14.68. Further work considering γ, σ_θ and its variability as parameters of the wind sea and individual swell trains could be done.

$$D(\theta) = \frac{2^{2s-1}}{\pi} \frac{\Gamma\left(s+1\right)^2}{\Gamma\left(2s+1\right)} \cos^{2s}\left(\frac{\theta - \theta_m}{2}\right), \tag{9}$$

$$s = \frac{2}{\sigma_\theta^2} - 1, \tag{10}$$

$$\int_0^{2\pi} D(\theta) d\theta = 1, \tag{11}$$

Following this methodology, we have reconstructed both the hindcast and our emulated sea and swell trains, so that we are able to compare the complete reconstructed spectra. The reason to also reconstruct the hindcast from its partitions, is to truly validate the performance of the emulator against the hindcast and not only the performance of the partitioning and the spectral reconstruction. When reconstructing the hindcast from its partitions we have observed that although the bulk parameters of both original and reconstructed spectra get very similar values, the reconstructed spectral energy is smoother, which could lead to further differences in Figure 9 than just the ones associated to the hindcast against the emulator.

Figure 9 shows the results of comparing the reconstructed mean spectra from the hindcast and the emulator (upper panels), the one associated to each season (middle panels) and the anomalies conditioned to the different AWTs. For the comparison we are focusing on the frequencies up to 0.3 Hz, although results up to 0.5 Hz have been obtained. As it can be inferred from Figure 9, a good agreement between hindcast and emulated spectra is found. We are capable of correctly reproducing seasonality, with boreal winters accounting for the largest energies mostly concentrated on the north-eastern directions, while the lowest energies are observed during the months of September through November, when it is also more probable to have waves approaching Majuro from the north-west. Waves from the southern hemisphere are more probable during the boreal summer, when also the trade winds are less intense.

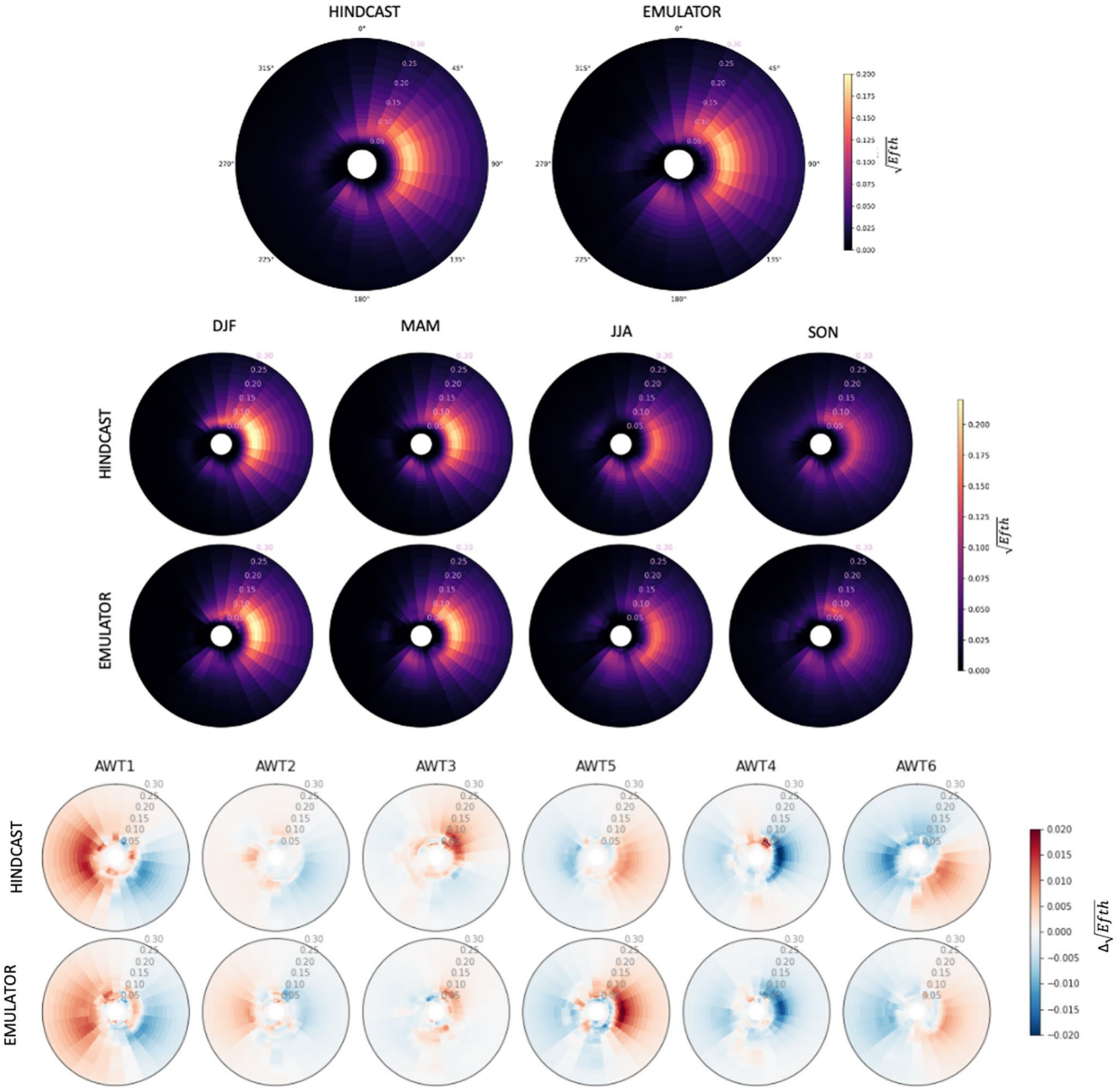

Figure 9. Comparison of hindcast against emulated spectra. Upper panels correspond to the annual mean, middle panels to the mean spectra associated to the different seasons and lower panels to the anomaly associated to the different AWTs.

Also, interannual variability is present in the emulated time series as observed in the lower panels of Figure 9, with the comparison against the hindcast. During El Niño (AWT1), we observe a negative anomaly of the energy coming from eastern directions, due to the weakening of the trade winds (Timmermann et al., 2018), and a positive anomaly of western seas, more common during El Niño events (Ford et al., 2018). The opposite behavior is observed during la Niña, when the most intense trade winds occur. The largest anomalies of swells, can be observed during El Niño, as in Figure 6.

Although we have discussed against the use of bulk parameters in these environments, they can still be useful for some applications and are a metric of the mean energy that needs to be correctly reproduced by the proposed climate-based emulator. For these reasons, and again using the library WAVESPECTRA, we have

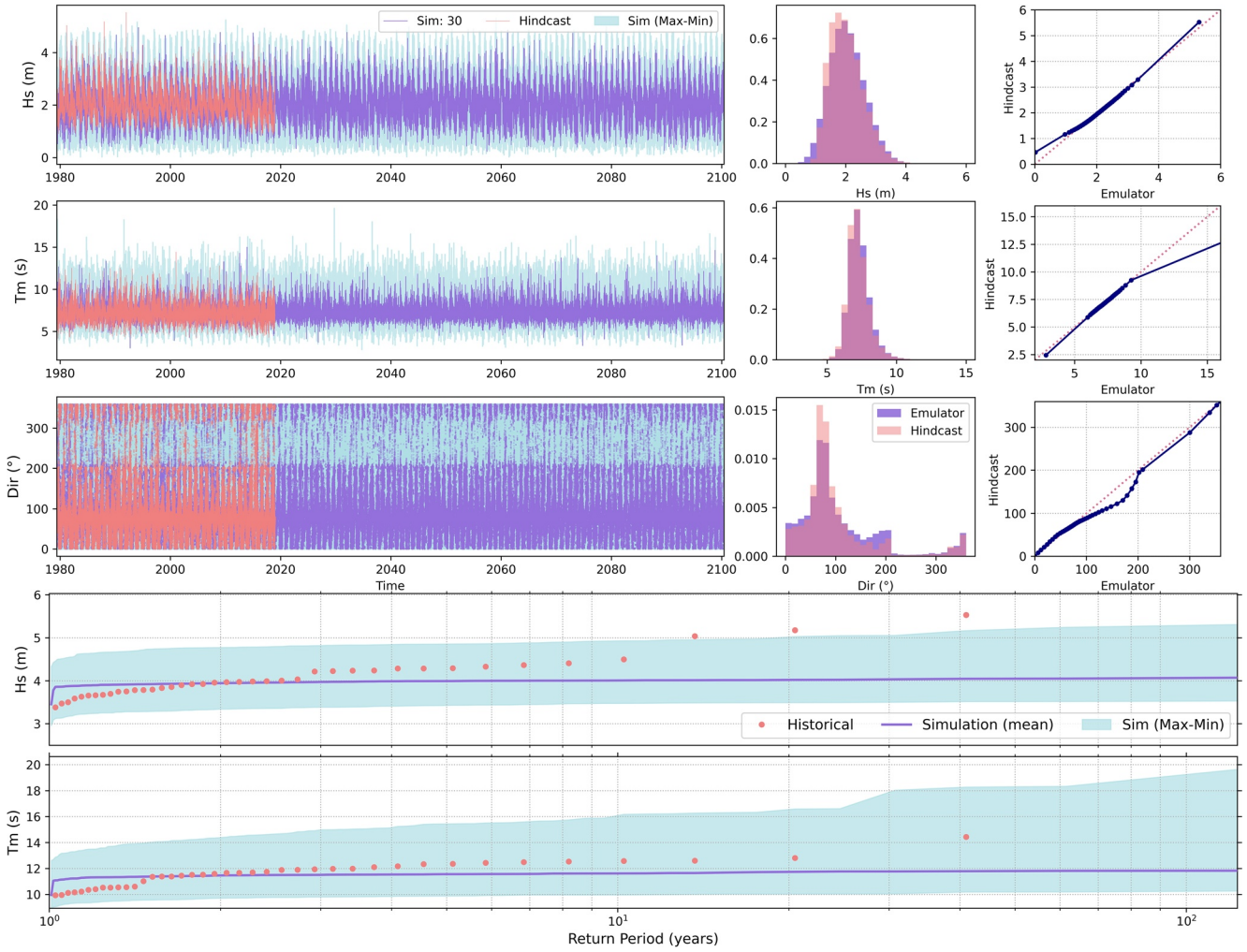

Figure 10. (Upper panels) Time series (left), histograms (middle), and qq-plots (right) of hindcasted and simulated bulk parameters. (Bottom panels) Return period of annual maxima of Hs and Tm; red dots represent hindcasted annual maxima, and the mean and maximum/minimum envelope of the simulations are represented in blue.

obtained the bulk parameters from the reconstructed spectra, and the comparison against the hindcast is shown on Figure 10. Here we are showing the time series of Hs, mean period (Tm) and Dir and comparing the mean distributions by means of histograms and Quantile-Quantile (QQ) plots. In the lower panels we also show the analysis associated to the return period of the annual maxima.

A general good agreement is found for both the mean and extreme wave regimes, although the most extreme Hs observed in the hindcast return period, are not reproduced by the climate emulator. The reason for the emulator to miss these events is that they are produced when a tropical storm (TS) is present, and more precisely typhoon Freda in March 1981, TS Roy in January 1988 and TS Axel in January 1992, for which damage to buildings and infrastructures was reported (Ford et al., 2018). The extraordinary characteristics and low probability of these events makes it not possible for the regular climate emulator to capture them, so future work in order to include the effect of tropical cyclones will be needed.

5. Discussion

Although there are different emulators proposed in the literature, this is the first to our knowledge to deal with the generation of synthetic independent swell trains and local seas, making it especially suitable for environments such as Pacific atolls where a sea and a number of swells do frequently occur at the same

time. A number of proposed emulators in recent years are based on the concept of splitting the atmospheric circulation into a number of synoptic patterns or weather types (WTs) at a daily scale (Anderson et al., 2019; Antolínez et al., 2016; Cagigal et al., 2020; Lucio et al., 2020; Rueda et al., 2017; Rueda, Camus, Méndez, et al., 2016; Rueda, Camus, Tomás, et al., 2016). Nevertheless, due to the purpose of their applications, some are limited to bulk wave parameters (Antolínez et al., 2016; Cagigal et al., 2020; Lucio et al., 2020).

The emulation of multimodal daily wave spectra was first introduced in Rueda et al. (2017), where the wave climate in California is divided into a sea and two different swells based on the generation regions. As storms generally have a duration larger than a day, to address the dependence between consecutive days, an extremal index was introduced, which allows to obtain accurate estimates of extremes but does not model the natural variability (Rueda, Camus, Tomás, et al., 2016; Rueda, Camus, Méndez, et al., 2016). Further improvements to account for the duration of each different storm were made in Anderson et al., (2019), where each storm is defined as the number of consecutive days with the same WT and is emulated by its peak and downscaled to hourly values following a trapezoidal shape for the different wave parameters. Nevertheless, the storm duration is constrained by the number of days with the same WT, and although the emulator is capable of reproducing a sea and two different swells associated with two defined generation areas, they all necessarily have the same duration.

In our analysis, we have observed that the different swell trains have different durations depending on their direction, as those approaching Majuro from the south tend to be longer than those approaching from the northern and eastern directions (Figure 5). Furthermore, it is very common to have more than one swell approaching the site from similar directions with different wave period at the same time. For these reasons, previously developed emulators are not enough to account for all these factors, and it is key to have a flexible emulator that allows the generation of individual swell trains, each with their own duration and characteristics over time, that also have the potential to overlap and interact with each other.

The ultimate purpose of this emulator is to be able of generating time series that better represent the natural processes of the multivariate wave climate in the Pacific region. The emulator proposed is relatively easy to construct and once it is optimized for each specific study site, it is not computational expensive and is able of generating infinitely long time series of individual swell trains and seas, which can ultimately be reconstructed to obtain hourly series of directional spectra. Even so, there are a number of key parameters on which a decision needs to be made in the process. First is the partitioning algorithm, for which the wind cut and age factor parameters need to be introduced. This is a key decision that affects the rest of the analysis, and, as discussed in Section 3.1, the objective is to avoid the continuous switch between the sea and swell partition, and correctly differentiate the far field generated swells from the locally generated waves. The parameters proposed are capable to accomplish this objective on different atolls in the Marshall Islands, as it is an area in which trade winds are constantly blowing and generating local waves that range between seas, young swells and mixed sea states. However, obtaining these parameters is not straightforward or universal. Also, as pointed out throughout the analysis, there are parameters that need to be optimized for the swell train detection algorithm. In this study, we have optimized mainly using the visual inspection of the results through an iterative trial and error process. However, more research is needed to optimize and automatize the obtention of these parameters in the future.

6. Conclusions

A new climate-based emulator is proposed on this work. The model is based on the analysis of all the spectral wave energy approaching our study site by aggregating the information from six hindcast points into a central super-point, which is then divided using a watershed algorithm into a sea and a number of swells. In order to isolate the different swell trains from a common source, we propose an algorithm that analyses the wave partitions bulk parameters over time and lately the isolated swell trains are parameterized. Using the link of the sea and the swell train parameters with the seasonality and ENSO variability, we are capable of ultimately creating an emulator that generates hourly multivariate wave spectra accounting from the seasonal to the interannual scale.

We envisage this emulator will be a useful tool for probabilistic assessments of coastal hazards and early warning systems in low-lying Pacific atolls, which are very vulnerable to coastal flooding in the present

and which will be even more affected in the coming years with the effect of climate change. The emulator allows to expand the historical records in order to capture all the different combinations of hydrodynamic conditions that could potentially lead to coastal flooding. Further research will have to be undertaken in order to couple the effect of tropical storms and tropical cyclones to the emulator of daily regular conditions.

Data Availability Statement

Spectral data was downloaded from: https://data-cbr.csiro.au/thredds/catalog.html. AWT information was obtained from Anderson et al. (2019). A repository with all the codes developed in Python and the different Jupyter Notebooks for its use and the visualization of results are provided at http://gitlab.com/geoocean/bluemath/climate-based-emulators/Snakes.

Acknowledgments
The authors would like to acknowledge CSIRO, for making the spectral hindcast data publicly available and Dylan Anderson for providing AWT information. This work would not have been possible without funding from the Spanish Ministry of Science and Innovation, project Beach4cast PID2019-107053RB-I00 and from the Strategic Environmental Research and Development Program-s grant DOD/SERDP RC-2644. LC is funded by a scholarship from the University of Auckland.

References

Aarnes, J., & Krogstad, H. E. (2001). *Partitioning sequences for the dissection of directional ocean wave spectra: A review. Part of work package* (Vol. 4, pp. 1–23). Retrieved from http://soprano.cls.fr/wp-uploads/2011/10/partitioningsequences.pdf

Anderson, D., Rueda, A., Cagigal, L., Antolinez, J. A. A., Mendez, F. J., & Ruggiero, P. (2019). Time-varying emulator for short and long-term analysis of coastal flood hazard potential. *Journal of Geophysical Research: Oceans*, *124*(12), 9209–9234. https://doi.org/10.1029/2019JC015312

Antolínez, J. A. A., Mendez, F. J., Camus, P., Vitousek, S., Gonzalez, M., Ruggiero, P., & Barnard, P. L. (2016). A multiscale climate emulator for long-term morphodynamics (MUSCLE-morpho), *Journal of Geophysical Research: Oceans*, *121*(1), 3261–3285. https://doi.org/10.1002/2015JC011107

Beetham, E., & Kench, P. S. (2018). Predicting wave overtopping thresholds on coral reef-island shorelines with future sea-level rise. *Nature Communications*, *9*(1), 1–8. https://doi.org/10.1038/s41467-018-06550-1

Ben Alaya, M. A., Chebana, F., & Ouarda, T. B. M. J. (2014). Probabilistic Gaussian copula regression model for multisite and multivariable downscaling. *Journal of Climate*, *27*(9), 3331–3347. https://doi.org/10.1175/JCLI-D-13-00333.1

Cagigal, L., Rueda, A., Anderson, D., Ruggiero, P., Merrifield, M. A., Montaño, J., et al. (2020). A multivariate, stochastic, climate-based wave emulator for shoreline change modeling. *Ocean Modelling*, *154*, 101695. https://doi.org/10.1016/j.ocemod.2020.101695

Callaghan, D. P., Nielsen, P., Short, A., & Ranasinghe, R. (2008). Statistical simulation of wave climate and extreme beach erosion. *Coastal Engineering*, *55*(5), 375–390. https://doi.org/10.1016/j.coastaleng.2007.12.003

Camus, P., Mendez, F. J., Medina, R., & Cofiño, A. S. (2011). Analysis of clustering and selection algorithms for the study of multivariate wave climate. *Coastal Engineering*, *58*(6), 453–462. https://doi.org/10.1016/j.coastaleng.2011.02.003

Cheriton, O., Storlazzi, C. D., & Rosenberger, K. J. (2016). Observations and estimates of wave-driven water level extremes at the Marshall. *Journal of Geophysical Research: Oceans*, *121*, 3121–3140. https://doi.org/10.1002/2015JC011231.Received

Delpey, M. T., Ardhuin, F., Collard, F., & Chapron, B. (2010). Space-time structure of long ocean swell fields. *Journal of Geophysical Research*, *115*(12), C12037. https://doi.org/10.1029/2009JC005885

Devaliere, E. M., Hanson, J. L., & Luettich, R. (2009). Spatial tracking of numerical wave model output using a spiral search algorithm. In *2009 WRI World Congress on Computer Science and Information Engineering, CSIE 2009* (Vol. 2, pp. 404–408). https://doi.org/10.1109/CSIE.2009.1021

Durrant, T., Greenslade, D., Hemar, M., & Trenham, C. (2014). *A Global hindcast focussed on the Central and South Pacific (technical report)*. CAWCR.

Ford, M., Merrifield, M. A., & Becker, J. M. (2018). Inundation of a low-lying urban atoll island: Majuro, Marshall Islands. *Natural Hazards*, *91*(3), 1273–1297. https://doi.org/10.1007/s11069-018-3183-5

Ford, M. R., & Kench, P. S. (2015). Multi-decadal shoreline changes in response to sea level rise in the Marshall Islands. *Anthropocene*, *11*, 14–24. https://doi.org/10.1016/j.ancene.2015.11.002

Genz, J., Aucan, J., Merrifield, M., Finney, B., Joel, K., & Kelen, A. (2009). Wave navigation in the Marshall Islands—Comparing indigenous and Western scientific knowledge of the ocean, *Oceanography*, *22*(2), 210–245. https://doi.org/10.5670/oceanog.2009.52

Gerling, T. W. (1992). Partitioning sequences and arrays of directional ocean wave spectra into component wave systems. *Journal of Atmospheric and Oceanic Technology*, *9*(4), 444–458. https://doi.org/10.1175/1520-0426(1992)009<0444:psaaod>2.0.co;2

Gesch, D., Palaseanu-Lovejoy, M., Danielson, J., Fletcher, C., Kottermair, M., Barbee, M., & Jalandoni, A. (2020). Inundation exposure assessment for Majuro atoll, Republic of the Marshall islands using a high-accuracy digital elevation model. *Remote Sensing*, *12*(1), 154. https://doi.org/10.3390/rs12010154

Goda, Y. (1999). A comparative review on the functional forms of directional wave spectrum. *Coastal Engineering Journal*, *41*(1–4), 1–20. https://doi.org/10.1142/s0578563499000024

Guanche, Y., Mínguez, R., & Méndez, F. J. (2014). Autoregressive logistic regression applied to atmospheric circulation patterns. *Climate Dynamics*, *42*(1–2), 537–552. https://doi.org/10.1007/s00382-013-1690-3

Hanson, J. L., & Phillips, O. M. (2001). Automated analysis of ocean surface directional wave spectra. *Journal of Atmospheric and Oceanic Technology*, *18*(2), 277–293. https://doi.org/10.1175/1520-0426(2001)018<0277:AAOOSD>2.0.CO;2

Hasselman, K., Barnett, T. P., Bouws, E., Carlson, H., Cartwright, D. E., Enke, K., et al. (1973). Measurements of wind-wave growth and swell decay during the Joint North Sea Wave Project (JONSWAP). *Erganzungsheft Zur Deutschen Hydrographischen Zeitschrift*, *46*.

Hastie, T., Tibshirani, R., & Friedman, J. (2001). *The elements of statistical learning*. New York, NY: Springer.

Hoeke, R. K., McInnes, K. L., Kruger, J. C., McNaught, R. J., Hunter, J. R., & Smithers, S. G. (2013). Widespread inundation of Pacific islands triggered by distant-source wind-waves. *Global and Planetary Change*, *108*, 128–138. https://doi.org/10.1016/j.gloplacha.2013.06.006

Hovmöller, B. E. (1949). The trough-and-ridge diagram. *Tellus*, *1*, 62–66. https://doi.org/10.3402/tellusa.v1i2.8498

Izaguirre, C., Méndez, F. J., Menéndez, M., & Losada, I. J. (2011). Global extreme wave height variability based on satellite data. *Geophysical Research Letters*, *38*(10), L10607. https://doi.org/10.1029/2011GL047302

Jiang, H. (2019). Spatially tracking wave events in partitioned numerical wave model outputs. *Journal of Atmospheric and Oceanic Technology*, *36*(10), 1933–1944. https://doi.org/10.1175/JTECH-D-18-0228.1

Kench, P. S., Thompson, D., Ford, M. R., Ogawa, H., & McLean, R. F. (2015). Coral islands defy sea-level rise over the past century: Records from a central Pacific atoll. *Geology*, *43*(6), 515–518. https://doi.org/10.1130/G36555.1

Kpogo-Nuwoklo, K. A., Olagnon, M., & Guédé, Z. (2014). Wave spectra partitioning and identification of wind sea and swell events. *Proceedings of the International Conference on Offshore Mechanics and Arctic Engineering—OMAE*. https://doi.org/10.1115/OMAE2014-24689

Kuik, A. J., van Vledder, G. P., & Holthuijsen, L. H. (1988). A method for the routine analysis of pitch-and-roll buoy wave data. *Journal of Physical Oceanography*, *18*, 1020–1034. https://doi.org/10.1175/1520-0485(1988)018<1020:amftra>2.0.co;2

Leonard, M., Westra, S., Phatak, A., Lambert, M., van den Hurk, B., Mcinnes, K., et al. (2014). A compound event framework for understanding extreme impacts. *Wiley Interdisciplinary Reviews: Climate Change*, *5*(1), 113–128. https://doi.org/10.1002/wcc.252

Lucio, D., Tomás, A., Lara, J. L., Camus, P., & Losada, I. J. (2020). Stochastic modeling of long-term wave climate based on weather patterns for coastal structures applications. *Coastal Engineering*, *161*, 103771. https://doi.org/10.1016/j.coastaleng.2020.103771

Marcos, M., Rohmer, J., Vousdoukas, M. I., Mentaschi, L., Le Cozannet, G., & Amores, A. (2019). Increased extreme coastal water levels due to the combined action of storm surges and wind waves. *Geophysical Research Letters*, *46*(8), 4356–4364. https://doi.org/10.1029/2019GL082599

Merrifield, M. A., Becker, J. M., Ford, M., & Yao, Y. (2014). Observations and estimates of wave-driven water level extremes at the Marshall Islands. *Geophysical Research Letters*, *41*(20), 7245–7253. https://doi.org/10.1002/2014GL061005

Mitsuyasu, H., Tasai, F., Suhara, T., Mizuno, S., Okhusu, M., Honda, T., & Rikiishi, K. (1975). Observations of the directional spectrum of ocean waves using a cloverleaf buoy. *Journal of Physical Oceanography*, *5*(4), 750–760. https://doi.org/10.1175/1520-0485(1975)005<0750:ootdso>2.0.co;2

Philander, S. G. H. (1983). El Niño (Southern oscillation). *Nature*, *302*, 295–301. https://doi.org/10.1038/302295a0

Pomeroy, A., Lowe, R., Symonds, G., Van Dongeren, A., & Moore, C. (2012). The dynamics of infragravity wave transformation over a fringing reef. *Journal of Geophysical Research*, *117*(11), C11022. https://doi.org/10.1029/2012JC008310

Portilla, J. (2012). Storm-source-locating algorithm based on the dispersive nature of ocean swells. *El Politécnico*, *4*(1), C2–C36.

Portilla, J., Cavaleri, L., & Van Vledder, G. P. (2015). Wave spectra partitioning and long term statistical distribution. *Ocean Modelling*, *96*, 148–160. https://doi.org/10.1016/j.ocemod.2015.06.008

Portilla, J., Ocampo-Torres, F. J., & Monbaliu, J. (2009). Spectral partitioning and identification of wind sea and swell. *Journal of Atmospheric and Oceanic Technology*, *26*(1), 107–122. https://doi.org/10.1175/2008JTECHO609.1

Reguero, B. G., Losada, I. J., & Méndez, F. J. (2019). A recent increase in global wave power as a consequence of oceanic warming. *Nature Communications*, *10*(1), 1–14. https://doi.org/10.1038/s41467-018-08066-0

Rueda, A., Camus, P., Méndez, F. J., Tomás, A., & Luceño, A. (2016). An extreme value model for maximum wave heights based on weather types. *Journal of Geophysical Research: Oceans*, *121*(2), 1262–1273. https://doi.org/10.1002/2015JC010952.Received

Rueda, A., Camus, P., Tomás, A., Vitousek, S., & Méndez, F. J. (2016). A multivariate extreme wave and storm surge climate emulator based on weather patterns. *Ocean Modelling*, *104*, 242–251. https://doi.org/10.1016/j.ocemod.2016.06.008

Rueda, A., Hegermiller, C. A., Camus, P., Vitousek, S., Ruggiero, P., Barnard, P. L., et al. (2017). Multiscale climate emulator of multimodal wave spectra: MUSCLE-spectra. *Journal of Geophysical Research: Oceans*, *121*(3), 2268–2285. https://doi.org/10.1002/2016JC011882.Received

Serafin, K. A., & Ruggiero, P. (2014). Simulating extreme total water levels using time-dependent, extreme value approach. *Journal of Geophysical Research: Oceans*, *119*, 6305–6329. https://doi.org/10.1002/2014JC010093.Received

Smith, G. A., Hemer, M., Greenslade, D., Trenham, C., Zieger, S., & Durrant, T. (2020). Global wave hindcast with Australian and Pacific Island Focus: From past to present. *Geoscience Data Journal*, *8*, 1–33. https://doi.org/10.1002/gdj3.104

Snodgrass, F. E., Groves, G. W., Hasselmann, K. F., Miller, G. R., Munk, W. H., & Powers, W. H. (1966). Propagation of ocean swell across the Pacific. *Philosophical Transactions of the Royal Society A: Mathematical, Physical and Engineering Sciences*, *259*(1103), 431–497.

Spada, G., Bamber, J. L., & Hurkmans, R. T. W. L. (2013). The gravitationally consistent sea-level fingerprint of future terrestrial ice loss. *Geophysical Research Letters*, *40*(3), 482–486. https://doi.org/10.1029/2012GL053000

Storlazzi, C. D., Gingerich, S. B., Van Dongeren, A., Cheriton, O. M., Swarzenski, P. W., Quataert, E., et al. (2018). Most atolls will be uninhabitable by the mid-21st century because of sea-level rise exacerbating wave-driven flooding. *Science Advances*, *4*(4), 1–10. https://doi.org/10.1126/sciadv.aap9741

Timmermann, A., An, S. I., Kug, J. S., Jin, F. F., Cai, W., Capotondi, A., et al. (2018). El Niño-Southern Oscillation complexity. *Nature*, *559*(7715), 535–545. https://doi.org/10.1038/s41586-018-0252-6

Tolman, H. L. (1991). A third-generation model for wind waves on slowly varying unsteady, and inhomogeneous depths and currents. *Journal of Physical Oceanography*, *21*, 782–797. https://doi.org/10.1175/1520-0485(1991)021<0782:atgmfw>2.0.co;2

Tracy, B., Devaliere, E., Hanson, J., Nicolini, T., & Tolman, H. (2007). Wind sea and swell delineation for numerical wave modeling. Paper presented at *10th International Workshop on Wave Hindcasting and Forecasting Coastal Hazard Symposium P12*. Retrieved from //publication/uuid/BDC84DF4-52C0-4FB7-AC88-5FBEDCE68D4F

Van Vledder, G. P. (2015). Swell-wave island interaction and piloting in the southern pacific ocean. In *36th IAHR World Congress*.

Vitousek, S., Barnard, P. L., Limber, P., Erikson, L., & Cole, B. (2017). A model integrating longshore and cross-shore processes for predicting long-term shoreline response to climate change. *Journal of Geophysical Research: Earth Surface*, *122*(4), 782–806. https://doi.org/10.1002/2016JF004065

Vitousek, S., Cagigal, L., Montaño, J., Rueda, A., Mendez, F., Coco, G., & Barnard, P. L. (2021). The application of ensemble wave forcing to quantify uncertainty of shoreline change predictions. *Journal of Geophysical Research: Earth Surface*, *126*, e2019JF005506. https://doi.org/10.1029/2019jf005506

Vousdoukas, M. I., Mentaschi, L., Voukouvalas, E., Verlaan, M., Jevrejeva, S., Jackson, L. P., & Feyen, L. (2018). Global probabilistic projections of extreme sea levels show intensification of coastal flood hazard. *Nature Communications*, *9*(1), 1–12. https://doi.org/10.1038/s41467-018-04692-w

Wahl, T., Mudersbach, C., & Jensen, J. (2012). Assessing the hydrodynamic boundary conditions for risk analyses in coastal areas: A multivariate statistical approach based on Copula functions. *Natural Hazards and Earth System Science*, *12*(2), 495–510. https://doi.org/10.5194/nhess-12-495-2012

Wandres, M., Aucan, J., Espejo, A., Jackson, N., Yeurt, A. D. R. N., Damlamian, H., & Silva, R. (2020). Distant-source swells cause coastal inundation on Fiji#x02010;s coral coast. *Frontiers in Marine Science*, *7*, 1–10. https://doi.org/10.3389/fmars.2020.00546

Winter, G., Storlazzi, C., Vitousek, S., vanDongeren, A., McCall, R., Hoeke, R., et al. (2020). Steps to develop early warning systems and future scenarios of storm wave-driven flooding along coral Reef-lined coasts. *Frontiers in Marine Science*, *7*, 1–8. https://doi.org/10.3389/fmars.2020.00199

Yahav, I., & Shmueli, G. (2007). *An elegant method for generating multivariate Poisson random variable*. Retrieved from http://arxiv.org/abs/0710.5670